Articles
doi.org/10.1002/batt.201900198

Chemistry Europe
European Chemical Societies Publishing

Special Collection

Towards Germanium Layered Materials as Superior Negative Electrodes for Li-, Na-, and K-Ion Batteries

Laura C. Loaiza,[a] Laure Monconduit,[b, c, d] and Vincent Seznec*[a, c, d]

The germanium high theoretical capacity renders it as a promising anode material with 1384 mAh/g for Li ($Li_{15}Ge_4$) and 369 mAh/g for Na (NaGe) and K (KGe). Nevertheless, Ge suffers from volume variations due to alkali insertion, to mitigate this issue several strategies have been proposed. Among them the use of layered Ge-based phases, obtained from the $CaGe_2$ Zintl phase by topotactic deintercalation of Ca^{2+} to form the germanane $(GeH)_n$. This last one has a particular morphology of Ge_6 rings interconnected to form planes that buffers the volume changes and shortens the diffusion pathways. Here, we have studied the germanane alkali storage properties and 2150, 495 and 205 mAh/g of reversible capacity were obtained for Li, Na and K, respectively. These results indicate that germanane can store more alkali ions than the predicted phases, perform well at high rates and maintain a good capacity retention.

1. Introduction

Nowadays, the batteries play a key role in almost all of the technologies that surround humankind. In order to satisfy the increasing demand, the design of more efficient devices with higher energy densities and cycle life is crucial. In this context group 14 elements appear as suitable candidates for anode materials due to their high theoretical capacities. Particularly, Ge forms $Li_{15}Ge_4$[1] with 1384 mAh/g and NaGe[2] and KGe[3] with 369 mAh/g. These significant specific capacity values come at the expense of a volume expansion that leads to a capacity fading. Additionally, Ge is less abundant than Si, thus its practical application remains hindered by its high cost. Nevertheless, it presents a series of advantages over silicon as an electrode: i) it allows very fast Li^+ diffusion, (ca 400 times faster than in silicon)[4,5] and exhibits an electronic conductivity two orders of magnitude larger.[6] ii) Lithiated Ge alloys have a slightly lower volumes than the corresponding Si analogues, hence their associated volumetric expansion is smaller.[7] iii) Ge experiences an isotropic volume expansion that permits a facile stress relaxation; while this process in Si is anisotropic and promotes the formation of cracks in the electrode.[8]

Several strategies have been proposed in the literature to mitigate the volume variations in Ge anode electrodes, among them, the reduction of the dimensions to form nanoparticles, nanowires, nanotubes and thin films.[9] Another option are the layered or two-dimensional materials (2D), in which the active surface area is increased and the energy barrier for diffusion is lower. For the group 14 the dimensional diversity is based in the nature of the bonding between atoms, producing Ge with layered structures based on a mix sp^2-sp^3 bonding with the fourth bond completed by –H or –OH, such in germanane $(GeH)_n$.[10] This last one is obtained from the layered $CaGe_2$ in which the [Ge^-] Zintl ion allows the topotactic deintercalation of Ca^{2+} while preserving the Ge backbone.[11] This germanium-based layered material was first reported in 2000[12,13] and presents several differences compared to its bulk counterpart, for instance it has a direct band gap and exhibit a strong photoluminescence (change in color from the gray-metallic in $CaGe_2$ to red in germanane[12]), which is directly related with the presence of –OH and –H groups.[14] Hence the nature of the ligands has a repercussion in the physical and chemical properties. This characteristic is absent in most of the Van der Waals compounds due to their neutrality, while for germanane it can be easily achieved by a modification of the synthesis conditions.[15] The germanane layers can be exfoliated into nanosheets (GeNS), by mechanical processes, like scotch tape or sonication.[16,17] These GeNS have buckled honeycomb structures identical to Ge (111) but are easily oxidized. This issue can be addressed by the introduction of covalent bonds improving the chemical and thermal stability.[18] This versatility of germanane sets it as promising candidate for battery applications, not only due to its layered structure and improved electronic conductivity and ion diffusivity but also by its feasibility to be modified to meet certain requirements; properties that undoubtedly would be beneficial for improving the electrochemical performance of Ge-based anodes in batteries. Other applications such as supercapacitors, optoelectronics or catalysis are foresee as well.

[a] Dr. L. C. Loaiza, Dr. V. Seznec
Université de Picardie Jules Verne
Laboratoire de Réactivité et Chimie des Solides (LRCS)
15 Rue Baudelocque, 80000 Amiens, France
E-mail: vincent.seznec@u-picardie.fr
[b] Dr. L. Monconduit
Institut Charles Gerhardt AIME
Université de Montpellier
Place Eugene Bataillon, Bat. 15, 34095 Montpellier Cedex 5, France
[c] Dr. L. Monconduit, Dr. V. Seznec
Réseau sur le Stockage Electrochimique de l'Energie (RS2E)
15 Rue Baudelocque, 80000 Amiens, France
[d] Dr. L. Monconduit, Dr. V. Seznec
ALISTORE European Research Institute
15 Rue Baudelocque, 80000 Amiens, France

Supporting information for this article is available on the WWW under https://doi.org/10.1002/batt.201900198

Special Collection An invited contribution to a Special Collection dedicated to the Symposium on Batteries and Supercapacitors at the E-MRS Spring Meeting 2019

In this study, the alkali-ion storage properties of germanane were evaluated, the results are very promising with 2150, 495 and 205 mAh/g of reversible capacity for Li, Na and K respectively. The layered morphology of germanane buffers the volume expansion, increases the surface area and lowers the energy barrier for diffusion.[17] These results show the versatility of germanane as anode material for different battery systems, opening the quest on a deeper research and understanding of the layered Ge-based phases.

2. Results and Discussion

2.1. $CaGe_2$

The $CaGe_2$ is a Zintl phase with a layered structure consisting of Ge_6 rings interconnected to form planes, each Ge atom is bonded to other 3 Ge atoms and completes the octet rule by accepting one electron from the Ca^{2+}. Likewise $CaSi_2$, the $CaGe_2$ phase presents several polymorphs (Figure S1). The β-$CaGe_2$ or 6R-$CaGe_2$, that crystallizes in the rhombohedral $CaSi_2$-type (space group R-3m), known for several decades as the only thermodynamically stable polymorph. Recent studies have revealed the existence of the 2H or α-$CaGe_2$ that crystallizes in a hexagonal cell (space group P63mc), its formation is related to the synthesis conditions and is a metastable phase stabilized by the presence of impurities.[19] The 3R-$CaGe_2$ has a rhombohedral unit cell (space group R-3m) and is the most stable polymorph at low temperature, while the 6R stabilizes above 673 K.[19] The aforementioned polymorphs mainly differ by their stacking sequences, the layers are organized in a staggered fashion, and follow the ABAB sequence for 2H-$CaGe_2$, ABC for 3R-$CaGe_2$ and AA'BB'CC' for 6R-$CaGe_2$.[20,21] The stacking compatibility allows the formation of other metastable phases, meaning that the 4H polymorph can be easily formed from the 3R-$CaGe_2$ by the addition of an A' stacking to the matrix.[19–21]

As observed in the Figure S1, the stacking originates different interlayer distances that are related to the $CaGe_2$ stability, indeed a large interlayer distance leads to a rapid decomposition upon contact with moisture, according to the reaction [Eq. (1)]:[22]

$$CaGe_2 + H_2O \rightarrow Ca(OH)_2(GeH)_2 \quad (1)$$

This decomposition product contains layers of germanane $(GeH)_n$ separated by $Ca(OH)_2$ monolayers with no destructive oxidation of the Ge backbone. The stacking sequence is preserved, although the c parameter is increased due to the bigger size of $Ca(OH)_2$.[20,23]

The $CaGe_2$ was synthesized by ball milling, mixing stoichiometric amounts of Ca and Ge followed by an annealing process at 800 °C in a sealed tube under Ar. The diffraction pattern and the corresponding Le Bail profile matching are presented in Figure 1-a. The analysis indicates the presence of at least two polymorphs, the 3R and 6R, but other polymorphs could be present. The annealing temperature (800 °C) allows the stabilization of both 3R and 6R, although if increased to 950 °C only the 6R should be formed. The profile matching provided refined cell parameters of $a/b = 4.008(2)$ Å, $c = 10.320(7)$ Å and $V = 143.64(1)$ Å^3 for the 3R-$CaGe_2$ and $a/b = 3.999(2)$ Å, $c = 30.714(3)$ Å and $V = 425.52(5)$ Å^3 for the 6R-$CaGe_2$, in line with the literature.[12,19,20,24] Likewise $CaSi_2$ the $CaGe_2$ presents a turbostratic disorder with a preferential orientation of the planes, impeding an adequate refinement.[20]

The Raman spectra for $CaGe_2$ (Figure 1-b), presented two A_{1g} modes at 300 and 202 cm^{-1} and three E_g modes at 244, 235 and 125 cm^{-1}. In layered hexagonal materials such as the 3R- and 6R-$CaGe_2$ the Eg modes correspond to the in-plane lattice vibrations while the A_{1g} to the out-of-plane.[24] In certain occasions some modes can be activated depending on the polarization of the incident light while some others are independent of this variable. The SEM pictures for the $CaGe_2$ showed in Figure 1-c indicate a layered morphology, with

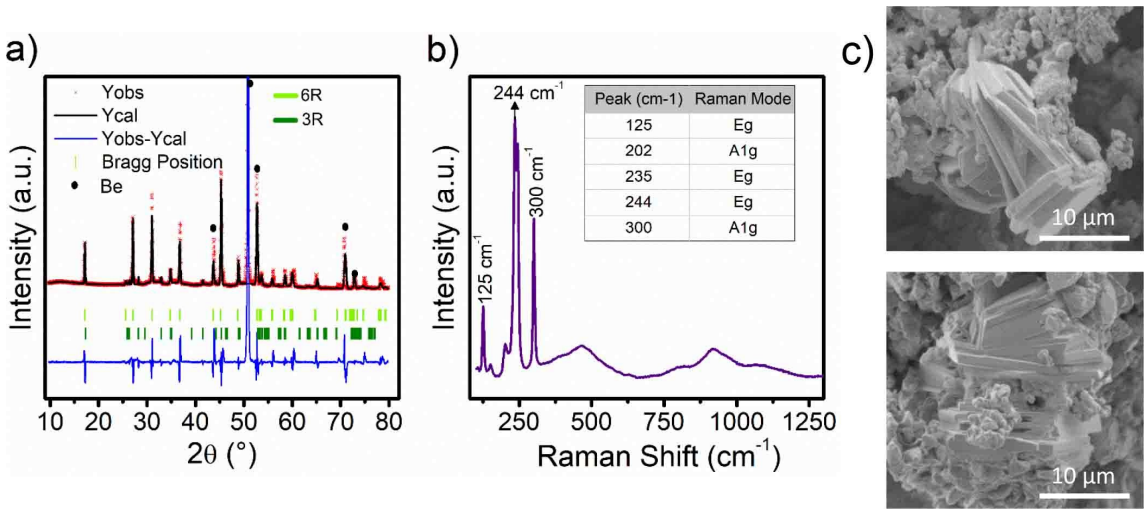

Figure 1. a) Le Bail profile matching for the $CaGe_2$ phase, **b)** Raman spectrum for $CaGe_2$, **c)** SEM pictures of the $CaGe_2$.

particles of different lateral size, agglomerates of several stacked layers and some particles with different morphology.

2.2. Germanane

The germanane was obtained from the $CaGe_2$, by dissolution in concentrated HCl at −20 °C, according to Equation 2. Contrary to siloxene,[25] the formation of germanane does not undergo a hydrolysis reaction even at temperatures >0 °C, yet the low temperatures increase the crystallinity.[12] Consequently germanane mainly forms Ge–H bonds and no Ge–OH, following the formula Ge_6H_6, which contrary to polysilane (Si_6H_6) is stable in air [Eq. (2)].[22] The resulting powder is reddish and exhibits photoluminescence in the infrared.[12]

$$3CaGe_2 + 6HCl + 3H_2O \rightarrow Ge_6H_6 + 3CaCl_2 + 3H_{2(g)} \quad (2)$$

The preferential bonding of Ge–H over Ge–OH reveals the different oxidation behavior of Si and Ge sheets. This difference can be understood in terms of the binding energies, the Si–O bond (8.0 eV) is significantly stronger than the Ge–O (6.6 eV) and the Si–H bond (3.0 eV) is slightly weaker than the Ge–H bond (3.2 eV). The absence of –OH bonds improves the germanane stability.[26] Nevertheless, the prolonged exposure to moisture causes substitution of Ge–H bonds by Ge–OH, forming the Germoxene $Ge_6OH_3H_3$. This compound has much less structural stability and the introduction of –OH groups predominately influences the band gap.[11,22]

Figure 2-a reveals the preservation of the layered morphology after the topotactic deintercalation of Ca in $CaGe_2$. The particle size distribution is inhomogeneous, various lateral sizes and stacks of different layers are observed. Indeed, the TEM images show the presence of several staggered layers as well as holes on the particle surface, probably caused by the H_2 released during the synthesis process.

The XRD pattern for germanane (Figure 2-c) is in line with the reports in the ICSD database (192507) for $(GeH)_n$. The broad diffraction peaks indicate a decrease in the crystallite size. The Le Bail profile matching shows the presence of two polymorphs, 3R-GeH and 6R-GeH, thus the crystal symmetry of $CaGe_2$ has been preserved after Ca deintercalation. The refined cell parameters of the 3R polymorph are a/b = 3.922(4)Å, c = 11.8764(7)Å and V = 158.2(9)Å^3, and for the 6R a/b = 4.027(9) Å, c = 34.6(1)Å and V = 486.9(3) Å^3 (Figure S2). Similarly to $CaGe_2$, the germanane presents an inherent turbostratic disorder that limits the quality of the refinement, although the obtained cell parameters are in line with the literature.[11,12,27] The *c* lattice constant expands from 10.320(7) Å in 3R-$CaGe_2$ to 11.8764(7) Å in 3R-GeH and from 30.714(3) Å in 6R-$CaGe_2$ to 34.6(1) Å in 6R-GeH. The *a* cell parameter experiences a slight decrease from 4.008(2) Å in $CaGe_2$ to 3.922(4) Å in germanane for the 3R polymorph, while for the 6R there is a slight increase from 3.999(2) Å in $CaGe_2$ to 4.027(9) Å in germanane, in agreement with the literature.[11,16,21] The expansion in the *c* parameter from $CaGe_2$ to germanane, is caused by the replacement of Ca^{2+} by two –H between each layer.[16] The interlayer distance d, calculated from the Bragg Equation, is 6.14 Å which is slightly lower than the one of siloxene 6.31 Å.[25] This decrease is related with the preferential bonding of germanane with –H and the almost absent –OH groups.[11,12] The electron diffraction (Figure 2-d) for germanane presents a high crystallinity and contrary to siloxene,[25] it is stable with the electron beam, thus the experiment can be performed under normal conditions. The pattern shows a preferential orientation of the planes and can be indexed in a hexagonal cell assuming a [011] zone axis.

Several polymorphs are reported for germanane: the 1T (P-3m1-one layer per trigonal unit cell), 2H ($P6_3mc$-two layers per hexagonal cell), 3R (R-3m three layers per rhombohedral cell), 4H (P-3m1 four layers per hexagonal cell) and 6R (R-3m six layers per rhombohedral cell). They all present a similar value for the *a* cell parameter, while the *c* varies according to the number of layers per unit cell.[11,21] Each polymorph present its

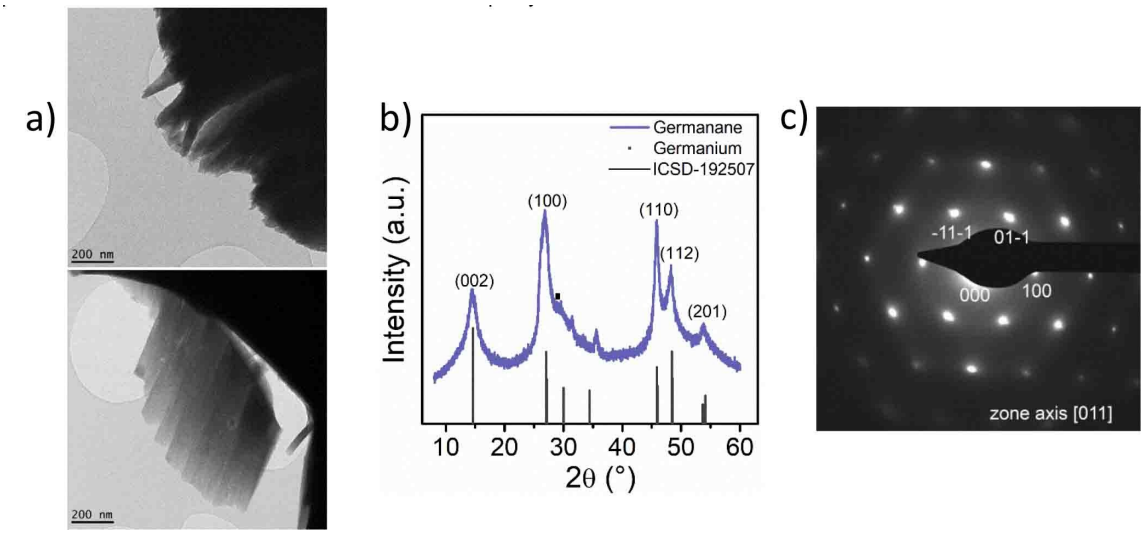

Figure 2. a) TEM picture of germanane, **b)** XRD diffraction pattern and **c)** Electron diffraction pattern for germanane.

stacking sequence, the 3R has ABC, the 4H A'ABC and the 6R A'AB'BC'C.[19] In analogy with $CaGe_2$ the interlayer distance is directly related to the staking sequence in the polymorph, the larger the distance is the highest is the reactivity.[11,19,27] Finally, several polymorphs can coexist in the same sample, thus in some cases their identification can be complex.[19]

The Raman spectrum (Figure 3-a) shows a change with respect to the $CaGe_2$, and it is composed of only one band centered at 302 cm^{-1} corresponding to the in-plane E_2 mode of the Ge–Ge bond. This signal is blue-shifted compared to the E_2 Ge–Ge signal for c-Ge centered at 297 cm^{-1}.[16] A similar band is observed in $CaGe_2$, corresponding to an out-of-plane A_{1g} vibration at 300 cm^{-1}. These results are in line with the literature, although the A_1 mode should be present at 227 cm^{-1}, probably the polarization of the incident light deactivates this Raman mode in our germanane. The Infrared spectrum in Figure 3-b, shows the presence of Ge–H vibrations, centered at 2000 cm^{-1} (Ge–H stretching) and 570 and 507 cm^{-1} (Ge–H wagging) preferentially oriented parallel to the *c* axis.[12] Other weak vibration modes are found at 770 and 850 cm^{-1}, assigned to the bending of $Ge–H_2$, probably located at the edges of the layers or originated from Ge vacancies.[16,26] The band at 830 cm^{-1} corresponds to the Ge–O–Ge stretching mode, indicating a partial oxidation of the planes or the presence of glassy/amorphous oxides. No –OH vibrations are found for germanane; thus the bonding is preferentially done with –H.

In order to evaluate the stability of germanane, an in situ controlled-temperature XRD was performed from 30 to 450 °C (Figure 4). The (002) and (100) Bragg reflections of germanane are present until 150 °C, temperature after which they shift towards higher angles and intensity decreases until complete disappearance at ~300 °C. Meanwhile, the peak at 27° assigned to c-Ge produced as a synthesis by-product and the additional small peaks from the Kapton window remain unchanged. According to the literature, the amorphization of germanane starts at 75 °C and is completed at 175 °C. The dehydrogenation occurs between 200–250 °C and at 300–350 °C the residual Cl from the synthesis is desorbed. Due to a stronger Si–H bonding compared with Ge–H, the dehydrogenation temperature for germanane is lower than the one of siloxene (400 °C).[12,16,28] The thermal stability of germanane can be improved by replacing the Ge–H bonds by the less reactive Ge-CH_3 ones.[15]

The electrochemical behavior of germanane was evaluated by galvanostatic cycling in Li, Na and K half-cells. The electrolyte was 1 M $LiFP_6$ ($NaPF_6$) in 1:1 EC/DMC + 1% FEC, while 0.8 M KPF_6 (KFSI) in 1:1 EC/DEC were used for potassium. Figure 5 shows the galvanostatic curves and their respective derivative curves. The discharge capacities for the first cycle are 3732, 982 and 485 mAh/g and for the second one 2150, 495 and 205 mAh/g for Li, Na and K, respectively. Note that the conductive additive contributes to the capacity with ~270 mAh/g for Li, ~120 mAh/g for Na and ~150 mAh/g for K (Figure S3). Surprisingly, the sodiation of germanane delivered a capacity that exceeds the theoretical capacity for NaGe (396 mAh/g), according to the literature more than one Na can be inserted in the Ge matrix.[29,30] For potassium, the optimal

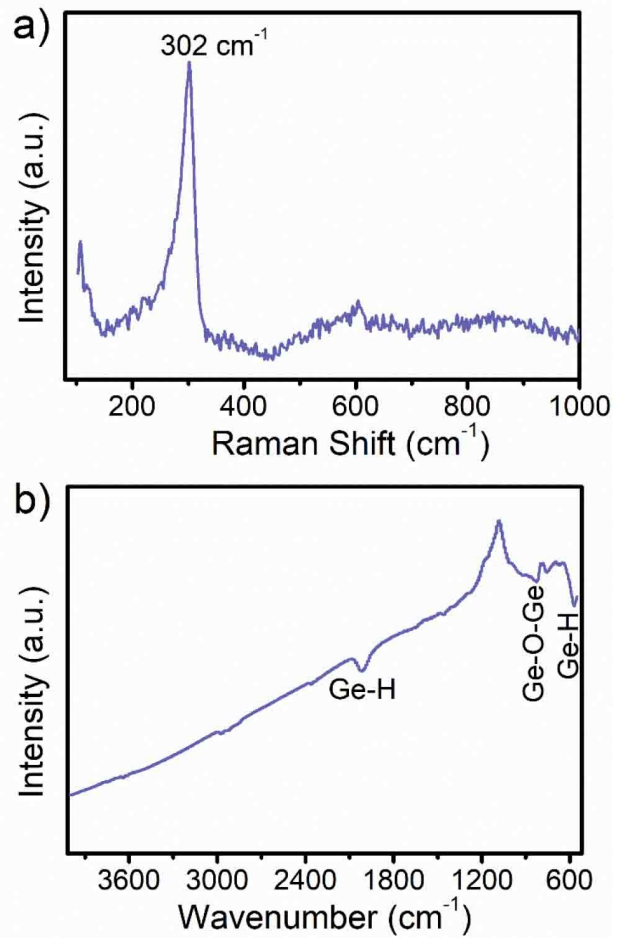

Figure 3. a) Raman and **b)** Infrared spectra for germanane.

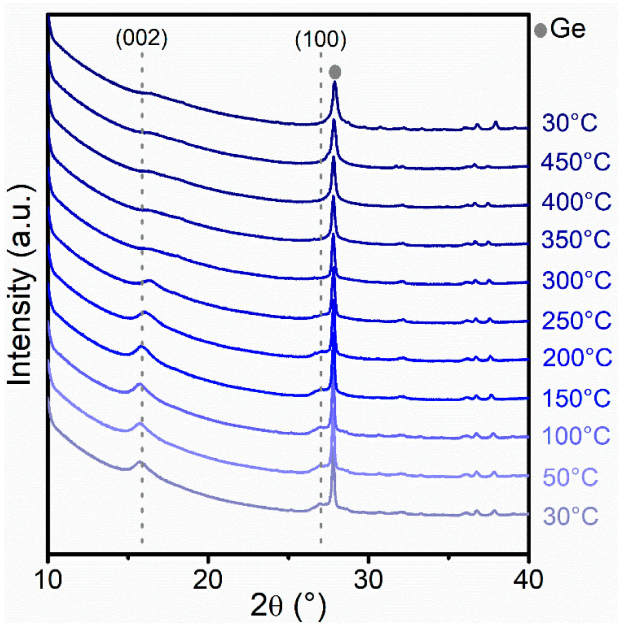

Figure 4. In situ XRD with temperature from 30–450 °C for germanane

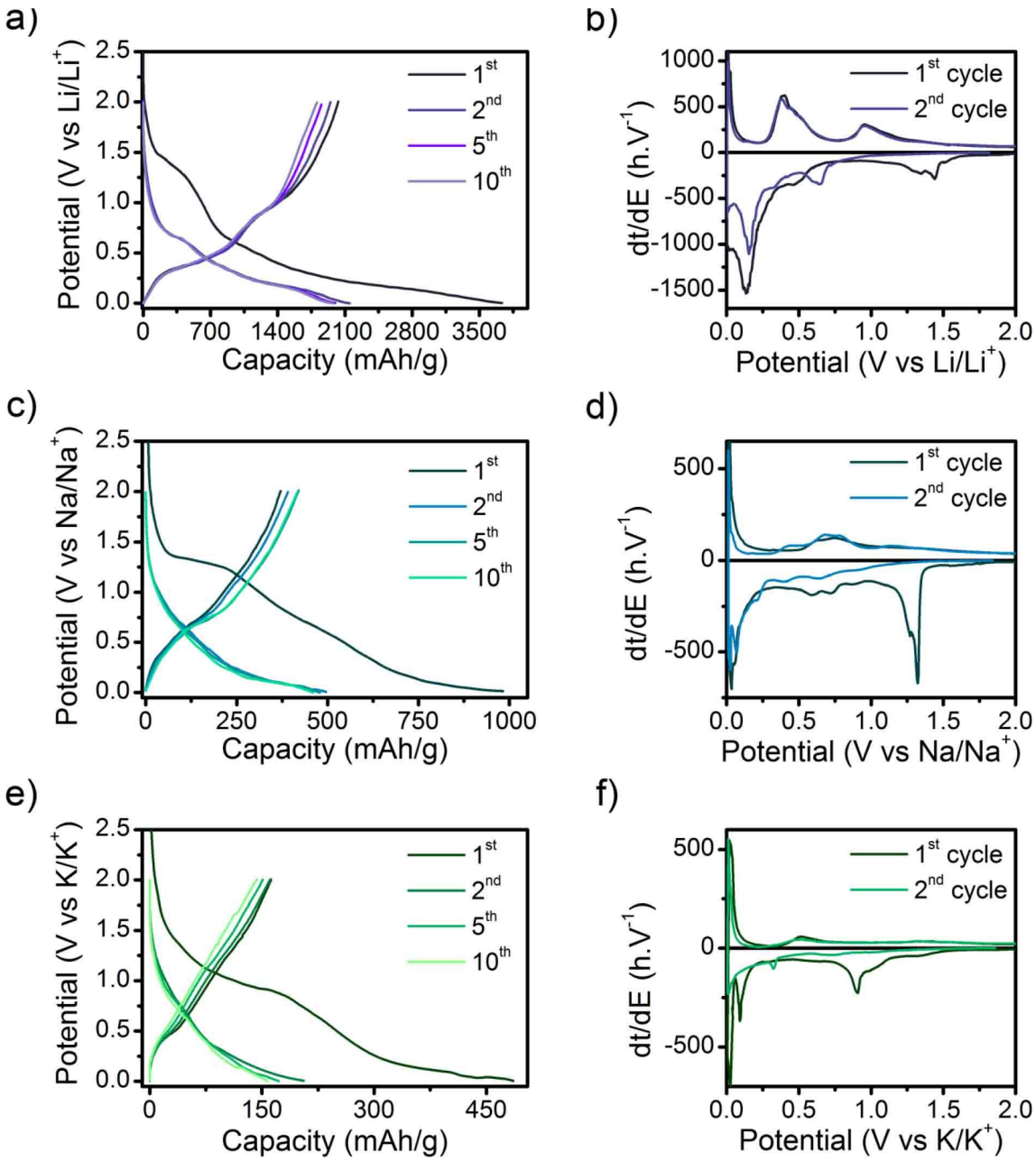

Figure 5. Galvanostatic curves and their respective derivative curves for the first cycle and second cycle for germanane vs **a**), **b**) Li, **c**), **d**) Na and **e**, **f**) K.

cycling conditions must be established before assuming an improved cyclability.

The galvanostatic cycling of germanane takes place at higher voltages compared to siloxene.[25] The first discharge for Li and Na is characterized by a plateau at ≈1.5 V and 1.3 V, respectively, assigned to the reduction of the FEC additive. Following, for Li there are two regions with different sloping profiles, the first one at around 0.6–0.3 V and the second one from 0.3–0 V. For the first charge and subsequent ones, two pseudo-plateaus are observed from 0.3–0.5 V and 0.5–1.0 V. The second discharge is slightly different from the first one, and a plateau is observed at 0.65 V, followed by a region with a sloping profile prolonged until 0.15 V. These features are reflected in the derivative curve (Figure 5-b) by a three reduction peaks at 1.2, 0.5 and 0.14 V during the first discharge, while the second one presented reduction peaks at 0.65 (plateau in the galvanostatic curve), 0.32 and 0.16 V. For the first and second oxidation, peaks at 0.4 and 0.95 V are observed, in line with the two-pseudo plateaus in the galvanostatic curve.

For sodium, in the first discharge after the plateau at 1.3 V, the potential decreases with a constant slope. For the first charge and subsequent ones, a pseudo-plateau is observed between 0.5–0.7 V, which gradually disappears as the cycling proceeds. The second discharge presents a constant sloping profile until 0.2 V followed by a steady decrease in the

potential. All these processes are displayed in the derivative curve (Figure 5-d), in the first discharge by reduction peaks at 1.3 and 0.04 V, accompanied by two other small signal at 0.6 and 0.7 V. For the first charge, one oxidation peak is observed at 0.7 V, in line with the pseudo-plateau in the galvanostatic curve. The second cycle, presents a double reduction peak at 0.08 and 0.04 V with a shoulder at 0.2 V, and an oxidation peak at 0.7 V with a shoulder at 0.4 V.

For potassium, the first discharge shows a very prolonged plateau at ≈1.0 V, followed by a gradual decrease in the voltage. Since this system has no FEC in the electrolyte formulation, this plateau must be attributed to another phenomenon than the reduction of FEC. The first and subsequent charge steps present a small region with a different slope approximately from 0.45–0.55 V that gradually vanishes with the cycling. The second discharge has a constant decrease in the voltage. The derivative curve (Figure 5-f) showed a reduction peak at 1.0 V, in line with the plateau in the galvanostatic curve, and two other peaks at 0.1 and 0.018 V during the first discharge. For the second discharge two reduction peaks are observed at 0.31 and 0.01 V. The first and second charge presents only one oxidation peak at 0.5 V.

The observed phenomena for the lithiation of germanane are in line with the only report available in the literature.[17] The galvanostatic curve presents a sloping profile. The derivative curve displays a broad reduction peak at 0.3 V and two oxidation ones at 0.5 and 0.9 V. Given the lack of information regarding the electrochemical mechanism of germanane, the source of these peaks remains unclear. The reported reversible capacities for germanane are in the range of 1108 mAh/g while for this work 2000 mAh/g were obtained at the same rate.[17]

Regarding the capacity retention properties (Figure 6), the germanane still delivers 1500, 354 and 150 mAh/g for Li, Na and K after 30, 35 and 30 cycles corresponding to a capacity retention of 67, 71 and 73%, respectively. Note that the capacity retention percentages are referred to the second cycle. The germanane showed great cyclability at high C/rates for Li as observed in Figure 6-b, where capacities in the range of 1100, 1000 and 900 mAh/g were delivered at C, 2 C and 5 C, respectively. This excellent rate capability can be attributed to the higher electron mobility in germanane compared to bulk Ge.[26] The sodiation of germanane is less accessible at high C/rates and 220, 170 and 120 mAh/g are obtained at C, 2 C and 5 C, respectively. At these rates, probably the capacity mainly comes from a capacitive behavior, as the Na ions do not have sufficient time to access the bulk of the layers, or from the conductive additive (120 mAh/g). Based on this information, the electrochemical behavior of germanane vs Li at high C/rates was tested, the results are presented in Figure 7.

As observed in Figure 7-a and Figure 7-b, the profile of the galvanostatic curve for germanane cycled at C and 2 C resembles to the one at C/10 described above, no significant changes, as polarization, are observed except for a size reduction of the plateau at 0.6 V during the second discharge for C and 2 C. The capacities for the first discharge were 2525 and 2383 mAh/g and for the second one 1560 and 1523 mAh/g for C and 2 C, respectively. A priori there is no major decrease in the capacity for C and 2 C during the first cycles. For instance, after 25 cycles 1130 mAh/g are delivered at 1 C and 2 C, corresponding to a capacity retention (with respect to the second cycle) of 72 and 74%, respectively. For the cell at 2 C after 58 cycles 990 mAh/g are obtained with a capacity retention of 65%. These values are higher compared to the reports in the literature, 530 and 265 mAh/g for 1 C and 2 C.[17] Thus, the germanane is very promising for high rate applications, for comparison siloxene presents a capacity retention of 52% after 58 cycles at 2 C. This improvement in germanane could be related with the almost 400 faster Li ion diffusion[5] and 2 orders of magnitude higher electronic conductivity[1] of Ge compared with Si.

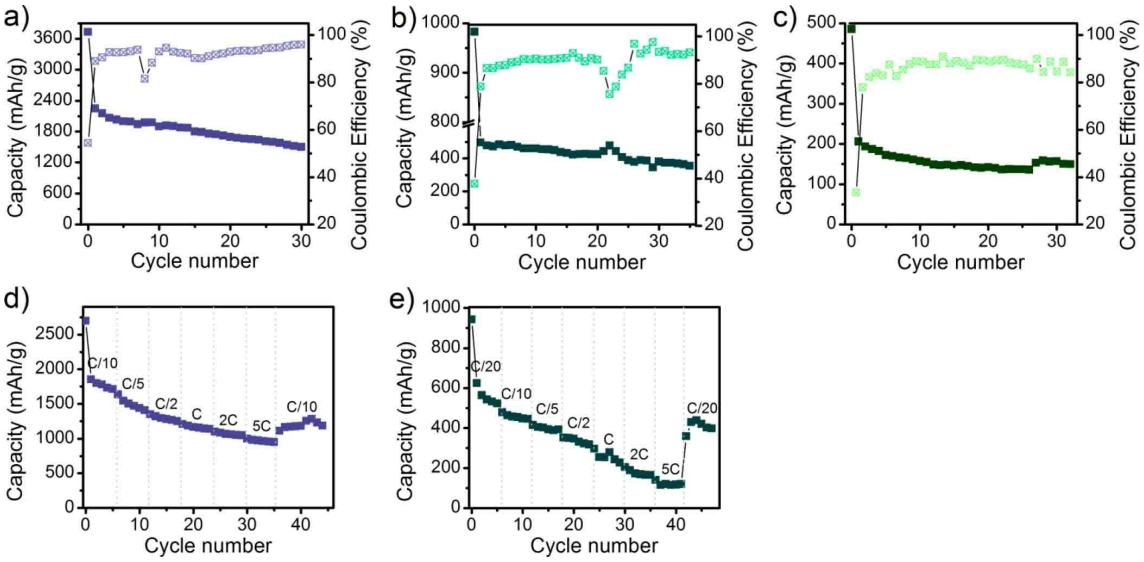

Figure 6. Capacity retention of germanane vs **a)** Li at C/10, b) Na and **c)** K at C/20. Rate performance at different C/rates for germanane vs d) Li and **e)** Na. The capacity values correspond to discharge capacity.

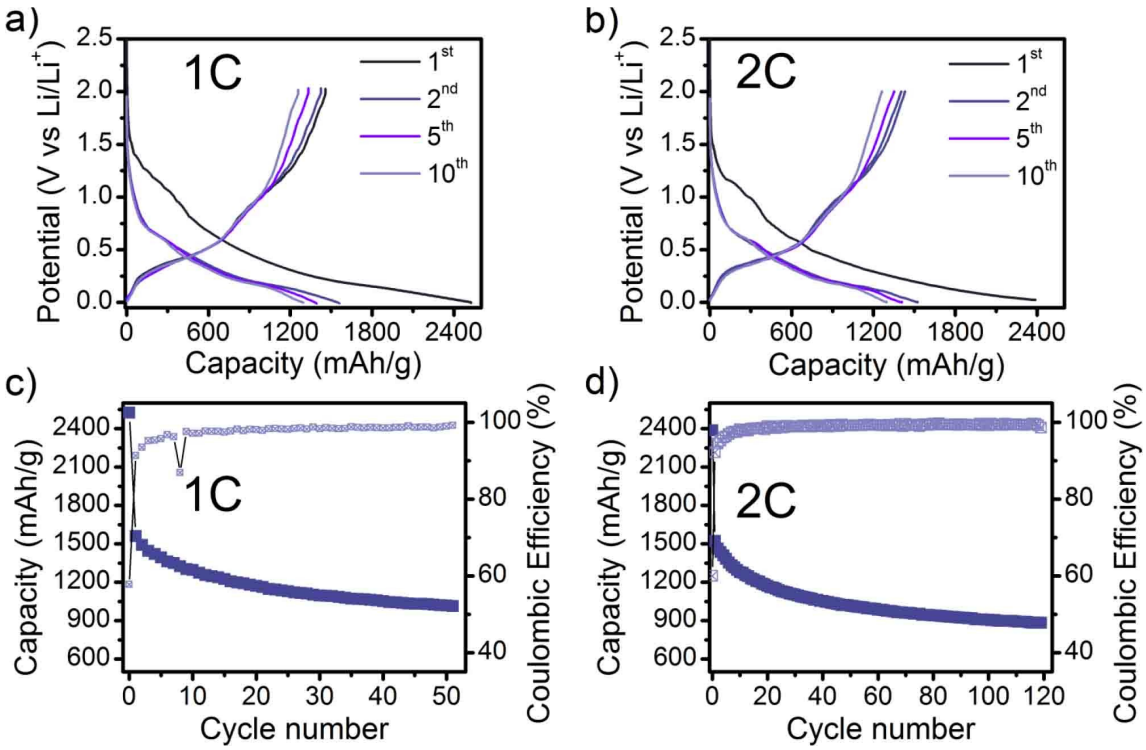

Figure 7. Galvanostatic and their corresponding capacity retention curves for germanane cycled vs Li at the rate of **a**), **c**) 1 C and **b**), **d**) 2 C.

The electrochemical behavior of bulk Ge and germanane were compared (Figure S4). In bulk Ge for the first discharge there is one plateau at 0.45 V, a pseudo plateau at about 0.2 V, reflected in the derivative curve by two reduction peaks at 0.43 and 0.14 V with a shoulder at 0.3 V. For the first and subsequent charge, there are two regions with a different slope between 0.3–0.5 V and 0.5–1.0 V, this last one gradually disappears with the cycling; only one oxidation peak is observed in the derivative curve at 0.43 V, accompanied by a shoulder for the second charge. The second discharge presents a plateau at 0.50 V and for the subsequent discharges the plateau appears at a higher potential 0.6 V. The derivative curve showed two reduction peaks at 0.48 and 0.14 V with a shoulder at 0.3 V. It is possible to observe then certain differences in the electrochemical behavior of germanane and bulk Ge; for the first discharge the germanane does not present the plateau and the reduction peak at 0.45 V, neither the shoulder at 0.3 V observed for bulk-Ge, while the peak at 0.14 V is present in both. For the charge, both materials share the oxidation peak at 0.43 V (region with different slope in the galvanostatic curve) and germanane presents an extra oxidation peak at 0.94 V (second pseudo plateau in the galvanostatic curve). These features are slight indicators of a different lithiation process, since the Ge is very sensitive to the cycling conditions. Probably due to the layered character of germanane the lithiated intermediates or even the electrochemical mechanism might be different. The germanane presented higher capacity values compared to bulk Ge, for both Li and Na (Figure S5). As expected the germanium presents an excellent capacity retention, property that is transferred to the germanane. This property along with the high reversible capacity renders germanane an excellent choice as anode material for Li-and Na-ion batteries.

Finally, the potassiation of germanane was evaluated (Figure S6), initially the same electrolyte formulation as for Li and Na was tested, 1 M KPF_6 in EC/DMC 1 %FEC and 1 M KFSI in EC/DMC 1 %FEC. The delivered capacities were 300 and 550 mAh/g for the formulation with KPF_6 and KFSI, respectively during the first discharge. The subsequent cycles are characterized by a remarked capacity loss and by the 5th cycle $<$ 50 mAh/g are obtained. Concerning the profile of the galvanostatic curve, in both cases a plateau at ~1.5 V is observed for the first discharge followed by a gradual decrease in the voltage until the end of discharge. The subsequent charge/discharge present an abrupt change in the voltage that is more pronounced as the cycling proceeds. Consequently, the germanane does not cycle correctly with K under these conditions.

Therefore alternative electrolyte formulations were proposed, 0.8 M KPF_6 in 1 : 1 EC/DEC and 0.8 M KFSI in 1 : 1 EC/DEC (Figure S7). The obtained capacities for the first discharge were 922 and 485 mAh/g for KPF_6 and KFSI, while the second discharge delivered respectively 202 and 205 mAh/g. For KPF_6 EC/DEC, the galvanostatic curve presents a sloping profile during the discharge/charge cycles. For KFSI EC/DEC a plateau at 1.0 V is observed during the first discharge and the subsequent charge/discharge cycles present a sloping profile. The cells cycled with KPF_6 EC/DEC presented more irreversibility and capacity fading compared to KFSI; and after 33 cycles only 56 mAh/g are delivered for KPF_6 in contrast to 150 mAh/g for KFSI. Therefore, as observed for siloxene, the formulation KFSI

in EC/DEC exhibits the best performance in terms of reversible capacity and capacity retention, though tests in full cell configuration are necessary to assess the real performance of germanane in KIB.

Finally, in order to get more information on the electrochemical kinetics, cyclic voltammetry has been performed on germanane. Figure 8-a, shows the CV curves for the first cycles of germanane, during the first cycle one reduction peak at 0.94 V and two oxidation ones at 0.47 and 1.06 V are observed. For the second cycle, there are three reduction peak at 0.55, 0.3 and 0.04 V while for oxidation two peaks at 0.45 and 1.1 V. The profile of the CV curve, evolves after the second cycle and a reduction peak at 0.32 V appears and the peak at 0.04 V is more defined and shifts to 0.08 V as the cycling proceeds. Meanwhile the oxidation peak gradually shifts to 0.43 V while the peak at approximately 1 V decreases in intensity. These processes are in line with the galvanostatic curve, in which two pseudo-plateaus are found upon discharge and charge. In general the profile of the CV curve for germanane suggests a good stability and reversibility for the system. Figure 8-b,c show the CV curves at different scan rates from 0.1 to 100 mV/s. For scan rates between 0.1 and 1 mV/s the CV curve displays the previously mentioned peaks, which become broader and less defined and the peak current increases with the scan rate. For scan rates from 10 to 100 mV/s, the peaks are very broad and the peak current continues to augment, indicating a high polarization.

The presence of capacitive or diffusion controlled processes was calculated from the relationship between the peak current (i_p) and the scan rate (v) [Eq. (3)]:[31]

$$i = av^b \tag{3}$$

Where b is determined by the slope between $log(i_p)$ vs $log(v)$ as in Figure 8-d. A b value of 0.5 indicates a diffusion controlled process while $b = 1$ represents a capacitive process. The b value obtained for germanane is 0.59 for both 0.1 to 1 mV/s and 5 to 100 mV/s. This value indicates that the storage mechanism is mainly diffusion controlled, in which the Faradic reaction occurs in the bulk of the material, with a smaller contribution from capacitive mechanism in which the storage only takes place at the surface of the layers and not in the bulk.[31]

As observed the electrochemical properties of germanane compared to bulk Ge for different alkali ions slightly differ, clearly the layered morphology and the conditions for cycling

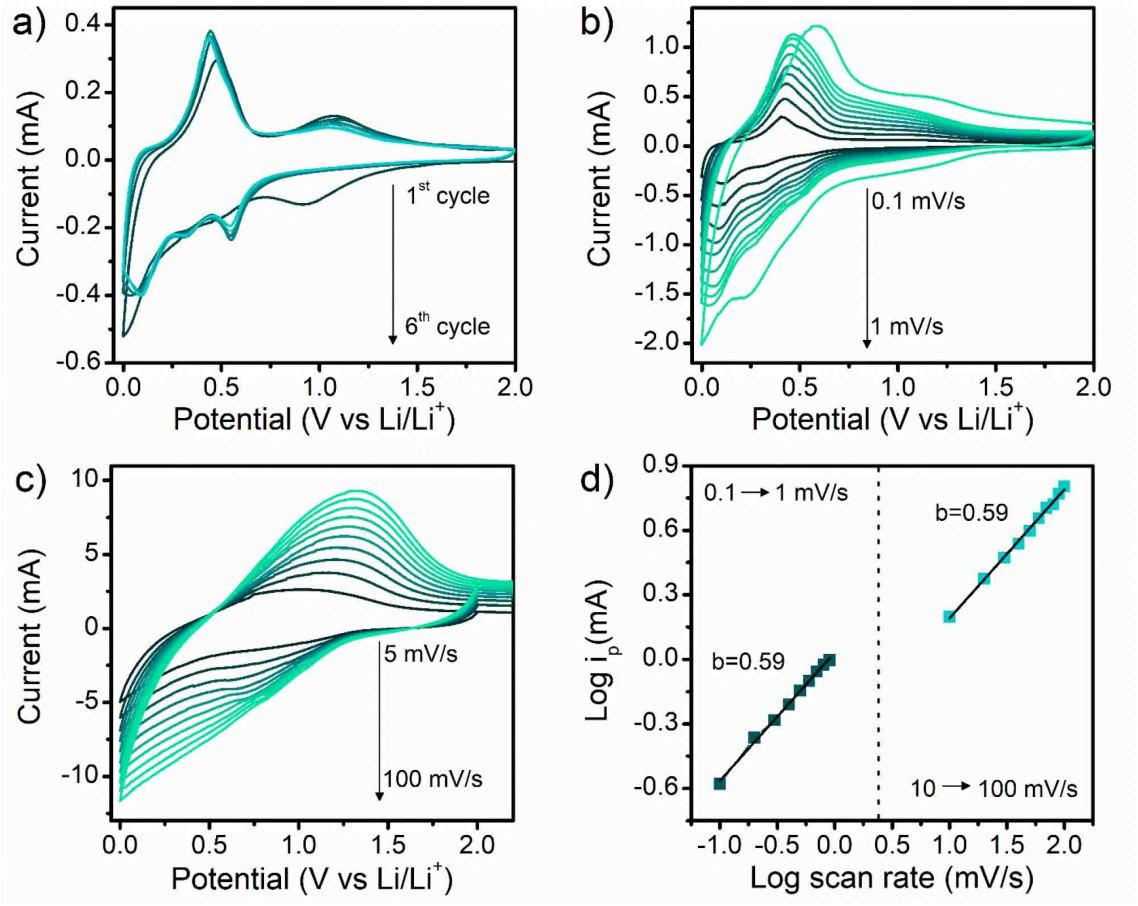

Figure 8. a) Cyclic voltammetry of germanane from first to sixth cycle at a scan rate of 0.1 mV/s. **b)** Cycling voltammetry at different scan rates from 0.1 mV/s to 1 mV/s. **c)** Cycling voltammetry at various scan rates from 5 mV/s to 100 mV/s. d) Determination of b-value using the relationship between the peak current and the scan rate.

might be involved. First, the layered morphology buffers the volume variations, reducing the strain due to reaction with alkali. Likewise, it provides faster diffusion paths for the alkali ions, allowing high rate applications. Secondly, recent studies indicate that Ge is particularly sensitive to the cycling conditions and parameters such as C/rate, morphology or electrode formulation can influence the type of phases that are formed. For instance in one of our previous studies for the lithiation of Ge, it was found that the cycling at relatively slow regime permits the stabilization of $Li_{17}Ge_4$, a more lithiated phase than $Li_{15}Ge_4$.[32] Another study concerning the sodiation of Ge Nanowires, has shown the formation of $Na_{1.6}Ge$, much sodiated phase than the expected NaGe.[2] These results put in evidence the influence of the different parameters involved in the cycling with the reversible capacities of Ge-based materials, the phases that are formed often differ from those ones commonly known, thus deeper studies are needed. In the case of germanane, the layered morphology not only buffers the volume changes but also allows to attain much higher reversible capacities compared to bulk Ge.

3. Conclusions

In summary, the germanium-based layered phase, the germanane, was obtained from the layered $CaGe_2$. After topotactic deintercalation of Ca^{2+}, the $CaGe_2$ transfers the same crystal symmetry to the germanane and two polymorphs were identified by XRD, the 3R (R-3m, 3 layers per rhombohedral unit cell) and 6R (R-3m, 6 layers per rhombohedral unit cell). The SEM and TEM analysis showed a layered morphology for both $CaGe_2$ and germanane. The Raman and infrared characterization indicate a preferential bonding of Ge with –H and almost no formation of Ge–OH. The presence of Ge–O–Ge bonds was identified and ascribed to a possible oxygen incorporation in the Ge planes or the formation of amorphous GeO_x as by-product of the reaction. The thermal stability of germanane was estimated to $\approx$250 °C, yet the amorphization starts at lower temperatures. The electrochemical performance of germanane was evaluated in Li, Na and K half-cells. The reversible lithiation capacities are in between 1700–2000 mAh/g while the sodiation between 400–500 mAh/g. These results are very promising and higher compared to bulk-Ge cycled under the same conditions. Particularly, the sodiation is higher compared to siloxene,[25] proving the feasibility of Na insertion into layered group 14-derivated phases. The germanane displayed good performance at high rates and at 1 C and 2 C capacities in the range of 1100–1200 mAh/g are obtained, values that are superior to the previous reports in the literature.[17] For the potassiation, the results are more ambiguous, the germanane seems to deliver good reversible capacities when the KFSI EC/DEC formulation is used, yet, tests in full cell configuration are necessary.

Finally, the layered morphology of germanane influences the electrochemical behavior by buffering or mitigating the volume expansion during cycling. The decrease in the irreversible capacity, remains a challenge, and understanding of the role of the –H groups in the first discharge and formation of the SEI layer is crucial at this stage. Additionally, due to its structure the lithiated/sodiation intermediates might be different and even another electrochemical mechanism could take place. For instance, the theoretical studies predict the absorption of Li and Na in the germanane layers with lower Li diffusion barriers (0.21–0.76 eV) than in siloxene (1.2 eV).[33,34] This work opens the quest for developing all the potential from the germanane as anode for LIB, NIB and KIB.

Experimental Section

Synthesis: The $CaGe_2$ Zintl phase was mechanically synthesized by placing stoichiometric amounts of Ca (99% ACROS Organics) and Ge (325-Mesh, 99%, ACROS Organics) in an airtight 50 mL WC jar, with a ball:mass ratio of 10:1. The jar was rotated at 600 rpm for 18 h, in a planetary ball mill (RETSCH PM 100). The recovered powder was loaded into stainless steel tubes sealed by Arc welding under Ar atmosphere and annealed for 50 h at 800 °C.

The germanene was synthesized in air atmosphere, by dissolving ~300 mg of $CaGe_2$ in ~30 mL of HCl (35% VWR Chemicals) at −20 °C for 8 hours. The reddish product was washed with distilled water and acetone, separated by centrifugation and vacuum dried for 30 min. All synthesis products were kept in an argon atmosphere to avoid further oxidation. Note that this synthesis method has been adapted from,[17] though in this work the ball milling of $CaGe_2$ prior the annealing process, clearly results in the absence of impurities such as CaO in $CaGe_2$ and in less residual c-Ge in germanane.

The Powder XRD patterns were recorded in a Bruker D8 Advanced diffractometer with Cu radiation ($\lambda1 = 1.54056$ Å, $\lambda2 = 1.54439$ Å), using an in situ cell with Be window described in Ref. [35]. The germanane diffractograms were collected with a zero background single Si crystal XRD sample holder. The diffraction patterns were refined using the Fullprof software. Confocal ex situ Raman Spectroscopy was performed using a DXR 2 Raman Microscope (Thermo-Fisher Scientific, 532-nm excitation). The samples were placed in a glass slide and sealed with Kapton tape in order to avoid exposure to air. The Fourier transformed Infrared Spectra (Nicolet IS10, Themo-Fisher Scientific) were performed using KBr methods, an airtight cell with NaCl window was used for air sensitive samples. Particle morphology, size and microstructure were studied by SEM (SEM-environmental FEI Quanta 200 FEG microscope) while the composition was determined by Energy Dispersive X-ray EDX (X INCA Oxford). TEM was performed in a TEM-FEI Tecnai F20 S-TWIN, operating at 200 kV fitted with a Gatan Image Filter Tridiem in post column. The electron diffraction patterns were obtained with Selected Area Electron Diffraction (SAED). The air sensitive samples were prepared in an Ar filled glove box and transferred to the TEM under an Ar flow.

In situ temperature-controlled XRD. The XRD with temperature were performed in a Bruker D8 Advanced diffractometer with Cu radiation ($\lambda1 = 1.54056$ Å, $\lambda2 = 1.54439$ Å) equipped with a HTK 1200 °C Anton Parr Chamber.

Electrode preparation. The electrodes were prepared with a 1:1:1 mass ratio of active material, carbon super C_{45} and Carboxyl Methyl Cellulose (CMC–DS = 0.9, $M_w = 700\,000$ Aldrich), dissolved in distilled water with 0.1% of Triton X dispersant. The slurry was casted into copper foil using a doctor blade (50 μm thickness) and dried at ambient conditions for one day. 11.1 mm disks were cut and dried under vacuum at 70 °C overnight.

Electrochemistry. The electrodes were tested in Li, Na and K half-cells using CR2032 coin cells, 1 M $LiPF_6$ ($NaPF_6$) in Ethylene Carbonate (EC)/Dimethyl Carbonate (DMC) [1:1] electrolyte with 1% Fluoro-ethylene carbonate (FEC) as additive, and a Whatman glass fiber separator (GF/ D, 675 μm). For K several electrolyte formulations and the impact of FEC addition were tested, 0.8 M KFSI in 1:1 EC/DEC, 0.8 M KFSI 1:1 EC/DMC, 0.8 M KPF_6 1:1 EC/DEC and 0.8 M KPF_6 1:1 EC/DMC. Galvanostatic cycling was performed at 25 °C between 0 and 2 V versus Li/Li^+, Na/Na^+ or K/K^+ at C/20 or C/10 (C/n = 1Li, Na or K/n h), using a VMP3 or MPG2 (Biologic) device.

Keywords: germanane · layered germanium · anode · batteries · energy storage

[1] H. Jung, P. K. Allan, Y. Y. Hu, O. J. Borkiewicz, X. L. Wang, W. Q. Han, L. S. Du, C. J. Pickard, P. J. Chupas, K. W. Chapman, A. J. Morris, C. P. Grey, *Chem. Mater.* **2015**.
[2] X. Lu, E. R. Adkins, Y. He, L. Zhong, L. Luo, S. X. Mao, C. M. Wang, B. A. Korgel, *Chem. Mater.* **2016**, *28*, 1236.
[3] Q. Yang, Z. Wang, W. Xi, G. He, *Electrochem. Commun.* **2019**, *101*, 68.
[4] K. C. Klavetter, S. M. Wood, Y. M. Lin, J. L. Snider, N. C. Davy, A. M. Chockla, D. K. Romanovicz, B. A. Korgel, J. W. Lee, A. Heller, C. B. Mullins, *J. Power Sources* **2013**, *238*, 123.
[5] J. Graetz, C. C. Ahn, R. Yazami, B. Fultz, *J. Electrochem. Soc.* **2004**, *151*, A698.
[6] H. Jung, P. K. Allan, Y. Y. Hu, O. J. Borkiewicz, X. L. Wang, W. Q. Han, L. S. Du, C. J. Pickard, P. J. Chupas, K. W. Chapman, A. J. Morris, C. P. Grey, *Chem. Mater.* **2015**, *27*, 1031.
[7] T. D. Bogart, A. M. Chockla, B. A. Korgel, *Curr. Opin. Chem. Eng.*, 286.
[8] S. W. Lee, I. Ryu, W. D. Nix, Y. Cui, *Extreme. Mech. Lett.* **2015**, *2*, 15.
[9] W. Li, X. Sun, Y. Yu, *Small Methods* **2017**, 1600037.
[10] T. Teshome, A. Datta, *J. Phys. Chem. C* **2017**, *121*, 15169.
[11] G. Vogg, M. S. Brandt, L. J.-P. Meyer, M. Stutzmann, Z. Hajnal, B. Szücs, T. Rauenheim, *MRS Symp. Proceed.* **2001**, *667*, 2.
[12] G. Vogg, M. S. Brandt, M. Stutzmann, *Adv. Mater.* **2000**, *12*, 1278.
[13] N. Liu, G. Bo, Y. Liu, X. Xu, Y. Du, S. X. Dou, *Small* **2019**, 1805147.
[14] L. J. P. Meyer, Z. Hajnal, T. Frauenheim, M. S. Brandt, G. Vogg, B. Szűcs, *Phys. Rev. B* **2001**, *64*, 1.
[15] S. Jiang, S. Butler, E. Bianco, O. D. Restrepo, W. Windl, J. E. Goldberger, *Nat. Commun.* **2014**, *5*, 1.
[16] E. Bianco, S. Butler, S. Jiang, O. D. Restrepo, W. Windl, J. E. Goldberger, *ACS Nano* **2013**, *7*, 4414.
[17] A. C. Serino, J. S. Ko, M. T. Yeung, J. J. Schwartz, C. B. Kang, S. H. Tolbert, R. B. Kaner, B. S. Dunn, P. S. Weiss, *ACS Nano* **2017**, *11*, 7995.
[18] H. Yu, T. Helbich, L. M. Scherf, J. Chen, K. Cui, T. F. Fa, B. Rieger, J. G. C. Veinot, *Chem. Mater.* **2018**, *30*, 2274.
[19] R. Yaokawa, A. Nagoya, K. Mukai, H. Nakano, *Acta Mater.* **2018**, *151*, 347.
[20] P. H. Tobash, S. Bobev, *J. Solid State Chem.* **2007**, *180*, 1575.
[21] N. D. Cultrara, Y. Wang, M. Q. Arguilla, M. R. Scudder, S. Jiang, W. Windl, S. Bobev, J. E. Goldberger, *Chem. Mater.* **2018**, *30*, 1335.
[22] M. S. Brandt, G. Vogg, M. Stutzmann, In *Silicon Chemistry: From the Atom to Extended Systems*; Jutzi, P.; Schubert, U., Eds.; Wiley-VCH Verlag GmbH & Co, 2007; pp. 194–213.
[23] G. Vogg, L. J. P. Meyer, C. Miesner, M. S. Brandt, M. Stutzmann, *Monatsh. Chem.* **2001**, *132*, 1125.
[24] M. Q. Arguilla, N. D. Cultrara, M. R. Scudder, S. Jiang, R. D. Ross, J. E. Goldberger, *J. Mater. Chem. C* **2017**, *5*, 11259.
[25] L. C. Loaiza, L. Monconduit, V. Seznec, *J. Power Sources* **2019**, *417*, 99.
[26] N. Sahoo Gopal, R. J. Esteves, V. D. Punetha, D. Pestov, I. U. Arachchige, J. T. J. MCLeskey, *Appl. Phys. Lett.* **2016**, *109*, 23507.
[27] X. Luo, E. Zurek, *J. Phys. Chem. C* **2015**, *120*, 793.
[28] S. Jiang, E. Bianco, J. E. Goldberger, *J. Mater. Chem. C* **2014**, *2*, 3185.
[29] Q. Wang, C. Zhao, Y. Lu, Y. Li, Y. Zheng, Y. Qi, X. Rong, L. Jiang, X. Qi, Y. Shao, D. Pan, B. Li, Y.-S. Hu, L. Chen, *Small* **2017**, *13*, 1701835.
[30] H. Wu, W. Liu, L. Zheng, D. Zhu, N. Du, C. Xiao, L. Su, L. Wang, *ChemistryOpen* **2019**, *8*, 298.
[31] X. Yu, S. Yun, J. S. Yeon, P. Bhattacharya, L. Wang, S. W. Lee, X. Hu, H. S. Park, *Adv. Energy Mater.* **2018**, *8*, 1.
[32] L. C. Loaiza, N. Louvain, B. Fraisse, A. Boulaoued, A. Iadecola, P. Johansson, L. Stievano, V. Seznec, L. Monconduit, *J. Phys. Chem. C* **2018**, *122*.
[33] D. K. Sharma, S. Kumar, A. Laref, S. Auluck, *Comput. Condens. Matter* **2018**, *16*, e00314.
[34] R. Bhuvaneswari, V. Nagarajan, R. Chandiramouli, *Mater. Res. Express* **2019**, *6*, 35504.
[35] M. Morcrette, Y. Chabre, G. Vaughan, G. Amatucci, J. B. Leriche, S. Patoux, C. Masquelier, J. M. Tarascon, *Electrochim. Acta* **2002**, *47*, 3137.

Manuscript received: December 3, 2019
Revised manuscript received: January 16, 2020
Accepted manuscript online: January 20, 2020
Version of record online: January 30, 2020